

CHORUS

This is the accepted manuscript made available via CHORUS. The article has been published as:

Frame-Dragging Vortexes and Tidal Tendexes Attached to Colliding Black Holes: Visualizing the Curvature of Spacetime

Robert Owen, Jeandrew Brink, Yanbei Chen, Jeffrey D. Kaplan, Geoffrey Lovelace, Keith D. Matthews, David A. Nichols, Mark A. Scheel, Fan Zhang, Aaron Zimmerman, and Kip S. Thorne

Phys. Rev. Lett. **106**, 151101 — Published 11 April 2011

DOI: [10.1103/PhysRevLett.106.151101](https://doi.org/10.1103/PhysRevLett.106.151101)

Frame-Dragging Vortexes and Tidal Tendexes Attached to Colliding Black Holes: Visualizing the Curvature of Spacetime

Robert Owen,¹ Jeandrew Brink,² Yanbei Chen,³ Jeffrey D. Kaplan,³ Geoffrey Lovelace,¹ Keith D. Matthews,³ David A. Nichols,³ Mark A. Scheel,³ Fan Zhang,³ Aaron Zimmerman,³ and Kip S. Thorne^{3,4}

¹Center for Radiophysics and Space Research, Cornell University, Ithaca, New York, 14853

²National Institute of Theoretical Physics, Private Bag X1 Matieland, Stellenbosch, South Africa, 7602

³Theoretical Astrophysics 350-17, California Institute of Technology, Pasadena, CA 91125

⁴Stellenbosch Institute for Advanced Study (STIAS), Wallenberg Research Centre at Stellenbosch University, Marais Street, Stellenbosch 7600, South Africa

When one splits spacetime into space plus time, the spacetime curvature (Weyl tensor) gets split into an “electric” part \mathcal{E}_{jk} that describes tidal gravity and a “magnetic” part \mathcal{B}_{jk} that describes differential dragging of inertial frames. We introduce tools for visualizing \mathcal{B}_{jk} (frame-drag vortex lines, their vorticity, and vortexes) and \mathcal{E}_{jk} (tidal tendex lines, their tendicity, and tendexes), and also visualizations of a black-hole horizon’s (scalar) vorticity and tendicity. We use these tools to elucidate the nonlinear dynamics of curved spacetime in merging black-hole binaries.

PACS numbers: 04.25.dg, 04.25.D-, 04.30.-w, 04.25.Nx

Introduction.— When one foliates spacetime with spacelike hypersurfaces, the Weyl curvature tensor $C_{\alpha\beta\gamma\delta}$ (same as Riemann in vacuum) splits into “electric” and “magnetic” parts $\mathcal{E}_{jk} = C_{\hat{0}j\hat{0}k}$ and $\mathcal{B}_{jk} = \frac{1}{2}\epsilon_{j\hat{p}q}C^{\hat{p}q}_{k\hat{0}}$ (see e.g. [1] and references therein); both \mathcal{E}_{jk} and \mathcal{B}_{jk} are spatial, symmetric, and trace-free. Here the indices are in the reference frame of “orthogonal observers” who move orthogonal to the space slices; $\hat{0}$ is their time component, $\epsilon_{j\hat{p}q}$ is their spatial Levi-Civita tensor, and throughout we use units with $c = G = 1$.

Because two orthogonal observers separated by a tiny spatial vector $\boldsymbol{\xi}$ experience a relative tidal acceleration $\Delta a_j = -\mathcal{E}_{jk}\xi^k$, \mathcal{E}_{jk} is called the *tidal field*. And because a gyroscope at the tip of $\boldsymbol{\xi}$ precesses due to frame dragging with an angular velocity $\Delta\Omega_j = \mathcal{B}_{jk}\xi^k$ relative to inertial frames at the tail of $\boldsymbol{\xi}$, we call \mathcal{B}_{jk} the *frame-drag field*.

Vortexes and Tendexes in Black-Hole Horizons.— For a binary black hole, our space slices intersect the 3-dimensional (3D) event horizon in a 2D horizon with inward unit normal \mathbf{N} ; so \mathcal{B}_{NN} is the rate the frame-drag angular velocity around \mathbf{N} increases as one moves inward through the horizon. Because of the connection between rotation and vorticity, we call \mathcal{B}_{NN} the horizon’s *frame-drag vorticity*, or simply its *vorticity*.

Because \mathcal{B}_{NN} is boost-invariant along \mathbf{N} [2], the horizon’s vorticity is independent of how fast the orthogonal observers fall through the horizon, and is even unchanged if the observers hover immediately above the horizon (the FIDOs of the “black-hole membrane paradigm” [3]).

Figure 1 shows snapshots of the horizon for two identical black holes with transverse, oppositely directed spins \mathbf{S} , colliding head on. Before the collision, each horizon has a negative-vorticity region (red) centered on \mathbf{S} , and a positive-vorticity region (blue) on the other side. We call these regions of concentrated vorticity *horizon vortexes*. Our numerical simulation [4] shows the four vortexes being transferred to the merged horizon (Fig. 1b), then re-

taining their identities, but sloshing between positive and negative vorticity and gradually dying, as the hole settles into its final Schwarzschild state; see the movie at <http://www.black-holes.org/headon05aa.html>.

Because \mathcal{E}_{NN} measures the strength of the tidal-stretching acceleration felt by orthogonal observers as they fall through (or hover above) the horizon, we call it the horizon’s *tendicity* (a word coined by David Nichols from the Latin *tendere*, “to stretch”). On the two ends of the merged horizon in Fig. 1b there are regions of strongly enhanced tendicity, called *tendexes*; cf. Fig. 5 below.

An orthogonal observer falling through the horizon carries an orthonormal tetrad consisting of her 4-velocity \mathbf{U} , the horizon’s inward normal \mathbf{N} , and transverse vectors \mathbf{e}_2 and \mathbf{e}_3 . In the null tetrad $\mathbf{l} = (\mathbf{U} - \mathbf{N})/\sqrt{2}$ (tangent to horizon generators), $\mathbf{n} = (\mathbf{U} + \mathbf{N})/\sqrt{2}$, $\mathbf{m} = (\mathbf{e}_2 + i\mathbf{e}_3)/\sqrt{2}$, and \mathbf{m}^* , the Newman-Penrose Weyl scalar Ψ_2 [5] is $\Psi_2 = (\mathcal{E}_{NN} + i\mathcal{B}_{NN})/2$. Here we use sign conventions of [6], appropriate for our $(-+++)$ signature.

Penrose and Rindler [7] define a complex scalar curvature $\mathcal{K} = \mathcal{R}/4 + i\mathcal{X}/4$ of the 2D horizon, with \mathcal{R} its intrinsic (Ricci) scalar curvature (which characterizes the horizon’s shape) and \mathcal{X} proportional to the 2D curl of its Hájíček field [8] (the space-time part of the 3D horizon’s extrinsic curvature). Penrose and Rindler show that $\mathcal{K} = -\Psi_2 + \mu\rho - \lambda\sigma$, where ρ , σ , μ , and λ are

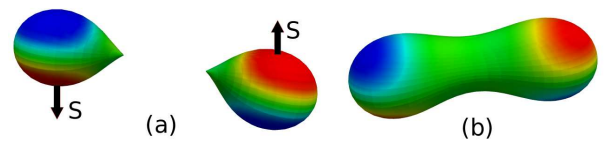


FIG. 1. Vortexes (with positive vorticity blue, negative vorticity red) on the 2D event horizons of spinning, colliding black holes, just before and just after merger. (From the simulation reported in [4].)

spin coefficients related to the expansion and shear of the null vectors \mathbf{l} and \mathbf{n} , respectively. In the limit of a shear- and expansion-free horizon (e.g. a quiescent black hole; Fig. 2a,b,c), $\mu\rho - \lambda\sigma$ vanishes, so $\mathcal{K} = -\Psi_2$, whence $\mathcal{R} = -2\mathcal{E}_{NN}$ and $\mathcal{X} = -2\mathcal{B}_{NN}$. As the dimensionless spin parameter a/M of a quiescent (Kerr) black hole is increased, the scalar curvature $\mathcal{R} = -2\mathcal{E}_{NN}$ at its poles decreases, becoming negative for $a/M > \sqrt{3}/2$; see the blue spots on the poles in Fig. 2b compared to solid red for the nonrotating hole in Fig. 2a. In our binary-black-hole simulations, the contributions of the spin coefficients to \mathcal{K} on the apparent horizons are small [$L2$ -norm $\lesssim 1\%$] so $\mathcal{R} \simeq -2\mathcal{E}_{NN}$ and $\mathcal{X} \simeq -2\mathcal{B}_{NN}$, except for a time interval $\sim 5M_{\text{tot}}$ near merger. Here M_{tot} is the binary's total mass. On the event horizon, the duration of spin-coefficient contributions $> 1\%$ is somewhat longer, but we do not yet have a good measure of it.

Because \mathcal{X} is the 2D curl of a 2D vector, its integral over the 2D horizon vanishes. Therefore, positive-vorticity regions must be balanced by negative-vorticity regions; it is impossible to have a horizon with just one vortex. By contrast, the Gauss-Bonnet theorem says the integral of \mathcal{R} over the 2D horizon is 8π (assuming S_2 topology), which implies the horizon tendicity \mathcal{E}_{NN} is predominantly negative (because $\mathcal{E}_{NN} \simeq -\mathcal{R}/2$ and \mathcal{R} is predominantly positive). Many black holes have negative horizon tendicity everywhere (an exception is Fig. 2b), so their horizon tendexes must be distinguished by deviations of \mathcal{E}_{NN} from a horizon-averaged value.

3D vortex and tendex lines—The frame-drag field \mathcal{B}_{jk} is symmetric and trace free and therefore is fully characterized by its three orthonormal eigenvectors $\mathbf{e}_{\bar{j}}$ and their eigenvalues $\mathcal{B}_{\bar{1}\bar{1}}$, $\mathcal{B}_{\bar{2}\bar{2}}$ and $\mathcal{B}_{\bar{3}\bar{3}}$. We call the integral curves along $\mathbf{e}_{\bar{j}}$ *vortex lines*, and their eigenvalue $\mathcal{B}_{\bar{j}\bar{j}}$ those lines' *vorticity*, and we call a concentration of vortex lines with large vorticity a *vortex*. For the tidal field \mathcal{E}_{jk} the analogous quantities are *tendex lines*, *tendicity* and *tendexes*. For a nonrotating (Schwarzschild) black hole, we show a few tendex lines in Fig. 2a; and for a rapidly-spinning black hole (Kerr metric with $a/M = 0.95$) we show tendex lines in Fig. 2b and vortex lines in Fig. 2c.

If a person's body (with length ℓ) is oriented along a positive-tendicity tendex line (blue in Fig. 2a), she feels a head-to-foot compressional acceleration $\Delta a = |\text{tendicity}|\ell$; for negative tendicity (red) it is a stretch. If her body is oriented along a positive-vorticity vortex line (blue in Fig. 2c), her head sees a gyroscope at her feet precess clockwise with angular speed $\Delta\Omega = |\text{vorticity}|\ell$, and her feet see a gyroscope at her head also precess clockwise at the same rate. For negative vorticity (red) the precessions are counterclockwise.

For a nonrotating black hole, the stretching tendex lines are radial, and the squeezing ones lie on spheres (Fig. 2a). When the hole is spun up to $a/M = 0.95$ (Fig. 2b), its toroidal tendex lines acquire a spiral, and its poloidal tendex lines, when emerging from one polar

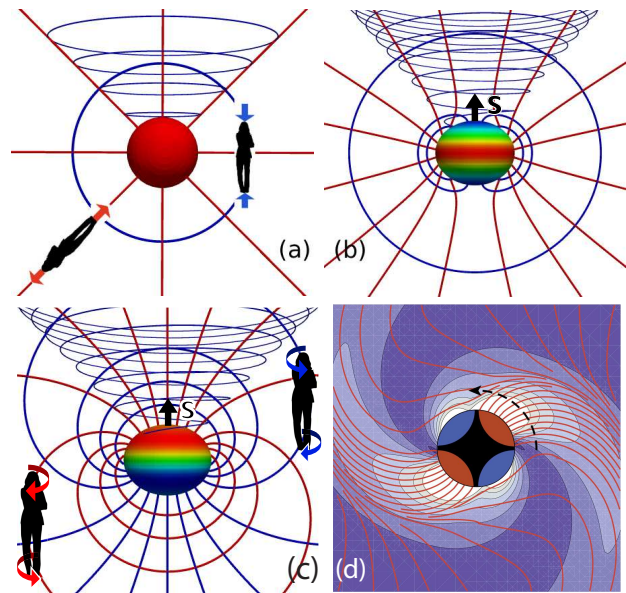


FIG. 2. Four different black holes, with horizons colored by their tendicity (upper two panels) or vorticity (lower two panels), ranging from most negative (red) to most positive (blue); and with a Kerr-Schild horizon-penetrating foliation (Exercise 33.8 of [9]). (a) A nonrotating black hole and its tendex lines; negative-tendicity lines are red, and positive blue. (b) A rapidly rotating (Kerr) black hole, with spin $a/M = 0.95$, and its tendex lines. (c) The same Kerr black hole and its vortex lines. (d) Equatorial plane of a nonrotating black hole that is oscillating in an odd-parity $l = m = 2$ quasinormal mode, with negative-vorticity vortex lines emerging from red horizon vortices. The lines' vorticities are indicated by contours and colors; the contour lines, in units $(2M)^{-2}$ and going outward from the hole, are $-10, -8, -6, -4, -2$.

region, return to the other polar region. For any spinning Kerr hole (e.g. Fig. 2c), the vortex lines from each polar region reach around the hole and return to the same region. The red vortex lines from the red north polar region constitute a *counterclockwise vortex*; the blue ones from the south polar region constitute a *clockwise vortex*.

As a dynamical example, consider a Schwarzschild black hole's fundamental odd-parity $l = m = 2$ quasinormal mode of pulsation, which is governed by Regge-Wheeler perturbation theory [10] and has angular eigenfrequency $\omega = (0.74734 - 0.17792i)/2M$, with M the hole's mass. From the perturbation equations, we have deduced the mode's horizon vorticity: $\mathcal{B}_{NN} = \Re\{9 \sin^2 \theta / (2i\omega M^3) \exp[2i\phi - i\omega(\tilde{t} + 2M)]\}$. (Here \tilde{t} is the ingoing Eddington-Finkelstein time coordinate, and the mode's Regge-Wheeler radial eigenfunction $Q(r)$ is normalized to unity near the horizon.) At time $\tilde{t} = 0$, this \mathcal{B}_{NN} exhibits four horizon vortices [red and blue in Fig. 2d], centered on the equator at $(\theta, \phi) = (\pi/2, 1.159 + k\pi/2)$ ($k = 0, 1, 2, 3$), and with central vorticities $\mathcal{B}_{NN} = -(-1)^k 39.22 / (2M)^2$. From analytic formulae for \mathcal{B}_{jk} and a numerical $Q(r)$, we have deduced the equatorial-plane

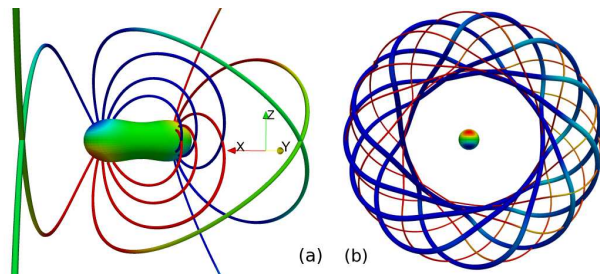


FIG. 3. Head-on, transverse-spin simulation: (a) Shortly after merger, vortex lines link horizon vortices of same polarity (red to red; blue to blue). Lines are color coded by vorticity (different scale from horizon). (b) Sloshing of near-zone vortices generates vortex loops traveling outward as gravitational waves; thick and thin lines are orthogonal vortex lines.

red vortex lines and vorticities shown in Fig. 2d. As time \tilde{t} passes, the vortices rotate counterclockwise, so they resemble water splayed out from a turning sprinkler. The transition from near zone to wave zone is at $r \sim 4M$ (near the outermost part of the second contour line). As one moves into the wave zone, each of the red vortices is smoothly transformed into a gravitational-wave trough and the 3D vortices that emerge from the blue horizon vortices (concentrated in the dark region of this figure) are transformed into gravitational-wave crests.

Vortex and Tendex Evolutions in Binary Black Holes (BBHs).— We have explored the evolution of frame-drag vortices and tidal tendexes in numerical simulations of three BBHs that differ greatly from each other.

Our first simulation (documented in [4]; movies at <http://www.black-holes.org/headon05aa.html>) is the head-on, transverse-spin merger depicted in Fig. 1 above, with spin magnitudes $a/M = 0.5$. As the holes approach each other then merge, their 3D vortex lines, which originally link a horizon vortex to itself on a single hole (Fig. 2c), reconnect so on the merged hole they link one horizon vortex to the other of the same polarity (Fig. 3a). After merger, the near-zone 3D vortices slush (their vorticity oscillates between positive and negative), generating vortex loops (Fig. 3b) that travel outward as gravitational waves.

Our second simulation (documented in [11]; movies at <http://www.black-holes.org/inspiral95aa.html>) is the inspiral and merger of two identical, fast-spinning holes ($a/M = 0.95$) with spins antialigned to the orbital angular momentum. Figure 4 shows the evolution of the vorticity \mathcal{B}_{NN} on the common apparent horizon beginning just after merger (at time $t/M_{\text{tot}} = 3483$), as seen in a frame that co-rotates with the small horizon vortices. In that frame, the small vortices (which arise from the initial holes' spins) appear to diffuse into the two large central vortices (which arise from the initial holes' orbital angular momentum), annihilating some of their vorticity. (This is similar to the diffusion and annihilation of mag-

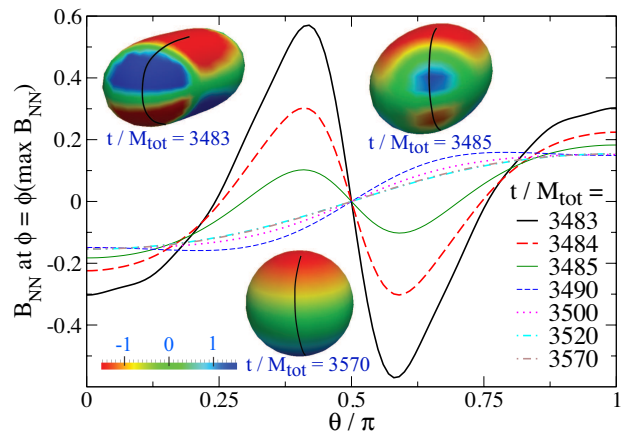


FIG. 4. Insets: snapshots of the common apparent horizon for the $a/M = 0.95$ anti-aligned simulation, color coded with the horizon vorticity B_{NN} . Graphs: B_{NN} as a function of polar angle θ at the azimuthal angle ϕ that bisects the four vortices (along the black curves in snapshots).

netic field lines with opposite polarity threading a horizon [3].) Making this heuristic description quantitative, or disproving it, is an important challenge.

Our third simulation (see movies at <http://www.black-holes.org/extreme-kick.html>) is a variant of the “extreme-kick” merger studied by Campanelli et al. [12] and others [13, 14]: two identical holes, merging from an initially circular orbit, with oppositely directed spins $a/M = 0.5$ lying in the orbital (x, y) plane. In this case, the vortices and tendexes in the merged hole’s (x, y) plane rotate as shown in Fig. 2d. We have tuned the initial conditions to make the final hole’s kick (nearly) maximal, in the $+z$ direction. The following considerations explain the origin of this maximized kick:

In a plane gravitational wave, all the vortex and tendex lines with nonzero eigenvalues lie in the wave fronts and make angles of 45 degrees to each other (bottom inset of Fig. 5.) For vectors \mathbf{E} (parallel to solid, positive-tendexity tendex line) and \mathbf{B} (parallel to dashed, positive-vorticity vortex line), $\mathbf{E} \times \mathbf{B}$ is in the wave’s propagation direction.

Now, during and after merger, the black hole’s near-zone rotating tendex lines (top left inset in Fig. 5) acquire accompanying vortex lines as they travel outward into the wave zone and become gravitational waves; and the rotating near-zone vortex lines acquire accompanying tendex lines. Because of the evolution-equation duality between \mathcal{E}_{ij} and \mathcal{B}_{ij} , the details of this wave formation are essentially the same for the rotating tendex and vortex lines. Now, in the near zone, the vectors \mathbf{E} and \mathbf{B} along the tendex and vortex lines (Fig. 5) make the same angle with respect to each other as in a gravitational wave (45 degrees) and have $\mathbf{E} \times \mathbf{B}$ in the $-z$ direction. This means that the gravitational waves produced by the rotating near-zone tendex lines and those produced by the rotating near-zone vortex lines will superpose constructively

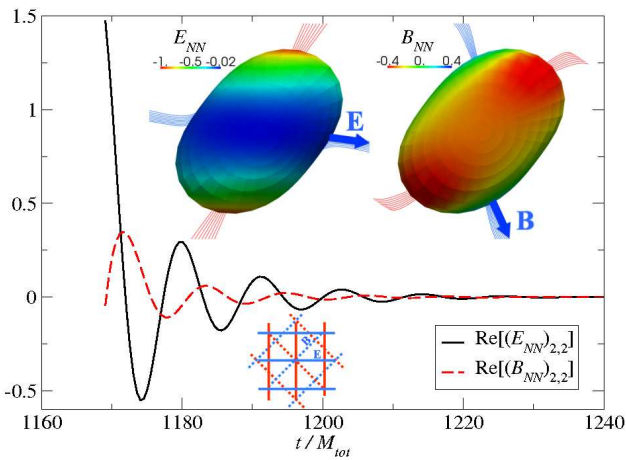


FIG. 5. Bottom inset: tendex and vortex lines for a plane gravitational wave; $\mathbf{E} \times \mathbf{B}$ is in the propagation direction. Upper two insets: for the “extreme-kick simulation”, as seen looking down the merged hole’s rotation axis ($-z$ direction): the apparent horizon color coded with the horizon tendicity (left inset) and vorticity (right inset), and with 3D vortex lines and tendex lines emerging from the horizon. The tendexes with the most positive tendicity (blue; \mathbf{E}) lead the positive-vorticity vortexes (blue; \mathbf{B}) by about 45° as they rotate counterclockwise. This 45° lead is verified in the oscillating curves, which show the rotating \mathcal{B}_{NN} and \mathcal{E}_{NN} projected onto a nonrotating $\ell = 2$, $m = 2$ spherical harmonic.

in the $-z$ direction and destructively in the $+z$ direction, leading to a maximized gravitational-wave momentum flow in the $-z$ direction and maximized black-hole kick in the $+z$ direction. An extension of this reasoning shows that the black-hole kick velocity is sinusoidal in twice the angle between the merged hole’s near-zone rotating vortexes and tendexes, in accord with simulations.

Conclusions.—In our BBH simulations, the nonlinear dynamics of curved spacetime appears to be dominated by (i) the transfer of spin-induced frame-drag vortexes from the initial holes to the final merged hole, (ii) the creation of two large vortexes on the merged hole associated with the orbital angular momentum, (iii) the subsequent sloshing, diffusion, and/or rotational motion of the spin-induced vortexes, (iv) the formation of strong negative \mathcal{E}_{NN} poloidal tendexes on the merged horizon at the locations of the original two holes, associated with the horizon’s elongation, and a positive \mathcal{E}_{NN} tendex at the neck where merger occurs, and (v) the oscillation, diffusion, and/or circulatory motion of these tendexes.

We *conjecture* that there is no other important dynamics in the merger and ringdown of BBHs. If so, there are important consequences: (i) This could account for the surprising simplicity of the BBH gravitational waveforms predicted by simulations. (ii) A systematic study of frame-drag vortexes and tidal tendexes in BBH simulations may produce improved understanding of BBHs, including their waveforms and kicks. The new waveform

insights may lead to improved functional forms for waveforms that are tuned via simulations to serve as templates in LIGO/VIRGO data analysis. (iii) Approximation techniques that aim to smoothly cover the full spacetime of BBH mergers (e.g. the combined Post-Newtonian and black-hole-perturbation theory method [15]) might be made to capture accurately the structure and dynamics of frame-drag vortexes and tidal tendexes. If so, these approximations may become powerful and accurate tools for generating BBH waveforms.

Acknowledgements.—We thank Larry Kidder and Saul Teukolsky for helpful discussions. Our simulations have been performed using the Spectral Einstein Code (SpEC) [16]. This research was supported by NSF grants PHY-0601459, PHY-0653653, PHY-0960291, PHY-0969111, PHY-1005426, and CAREER grant PHY-0956189, by NASA grants NNX09AF97G and NNX09AF96G, and by the Sherman Fairchild Foundation, the Brinson Foundation, and the David and Barbara Groce fund.

-
- [1] R. Maartens and B. A. Bassett, *Class. Quantum Grav.* **15**, 705 (1998).
 - [2] R. H. Price and K. S. Thorne, *Phys. Rev. D* **33**, 330915 (1986).
 - [3] K. S. Thorne, R. H. Price, and D. A. MacDonald, *Black Holes: The Membrane Paradigm* (Yale University Press, New Haven and London, 1986).
 - [4] G. Lovelace, Y. Chen, M. Cohen, J. D. Kaplan, D. Koppel, K. D. Matthews, D. A. Nichols, M. A. Scheel, and U. Sperhake, *Phys. Rev. D* **82**, 064031 (2010).
 - [5] E. Newman and R. Penrose, *Journal of Mathematical Physics* **3**, 566 (1962).
 - [6] V. P. Frolov and I. D. Novikov, *Black Hole Physics: Basic Concepts and New Developments* (Kluwer, 1998).
 - [7] R. Penrose and W. Rindler, *Spinors and Space-time, Volume 1* (Cambridge University Press, Cambridge, 1992).
 - [8] T. Damour, in *Proceedings of the Second Marcel Grossman Meeting on General Relativity*, edited by R. Ruffini (North-Holland Publishing Company, Amsterdam, 1982), pp. 587–606.
 - [9] C. W. Misner, K. S. Thorne, and J. A. Wheeler, *Gravitation* (Freeman, New York, New York, 1973).
 - [10] S. Chandrasekhar and S. Detweiler, *Proc. R. Soc. A* **344**, 441 (1975).
 - [11] G. Lovelace, M. A. Scheel, and B. Szilagyi, *Phys. Rev. D* **83**, 024010 (2011), arXiv:1010.2777.
 - [12] M. Campanelli, C. O. Lousto, Y. Zlochower, and D. Merritt, *Phys. Rev. Lett.* **98**, 231102 (2007), gr-qc/0702133.
 - [13] J. A. Gonzalez, M. D. Hannam, U. Sperhake, B. Brüggemann, and S. Husa, *Phys. Rev. Lett.* **98**, 231101 (2007), gr-qc/0702052.
 - [14] C. O. Lousto and Y. Zlochower, *Phys. Rev. D.* **83**, 024003 (2011), arXiv:1011.0593.
 - [15] D. A. Nichols and Y. Chen, *Phys. Rev. D* **82**, 104020 (2010).
 - [16] <http://www.black-holes.org/SpEC.html>.